Structure and magnetic properties of Co-doped ZnO nanoparticles

B. Martínez, F. Sandiumenge, and Ll. Balcells
Institut de Ciència de Materials de Barcelona (ICMAB-CSIC), Campus Universitari de Bellaterra, Bellaterra 08193, Spain

J. Arbiol
Serveis Cientifics, Univeristat de Barcelona, Diagonal 560, Barcelona 08028, Spain

F. Sibieude and C. Monty
CNRS/Institut de Science et Génie des Matériaux et Procédés, BP5 Odeillo, 66125-cedex Font Romeu, France

In this work we carefully analyze the role of the microstructure on the magnetic properties of Co-doped ZnO nanoparticles prepared by the vaporization-condensation method in a solar reactor. We show that a close correlation exists between microstructural features and the appearance of ferromagnetism. Both shape and size of the particles, as well as the microstructure, can be controlled by changing the pressure inside the evaporation chamber, as evidenced by transmission electron microscopy micrographs and high resolution electron microscopy (HREM). X-ray diffraction patterns and HREM make evident the absence of any significant Co segregation or any other phase different from würtzite type ZnO. On the other hand, electron energy loss spectroscopy analyses performed on several particles of würtzite type ZnO yielded an average Co concentration in good agreement with the nominal composition. Samples prepared in low pressure (≈ 10 Torr) exhibit a very homogeneous microstructure and are ferromagnetic at low temperature but they have a very small saturation moment, well below that expected for a Co^{2+} ion. Conversely, samples prepared at higher pressure conditions ($\approx 70-100$ Torr) show a defective microstructure and are paramagnetic and increasing the Co content does not induce ferromagnetism.

INTRODUCTION

Diluted magnetic semiconductors (DMS) have been the subject of recent interest due to their promising magnetic properties, since they make it possible to accommodate both charge and spin degrees of freedom in the same material. Their interplay is expected to allow the study of phenomena and the design of electronic devices with enhanced functionalities.[1,2] Even though the interest was initially centered on the group III arsenides and related materials, due to their immediate adaptation to the already existing semiconductors technology, the low values of the magnetic transition temperatures, T_C, found made clear the need for new materials with higher T_C. An important step forward in the field was the prediction by Dietl *et al.*[3] of high temperature ferromagnetism (FM) in some magnetically doped wide band-gap *p*-type semiconductors. Since then much attention has been focused on these materials. Particularly TiO_2 (Refs. 4 and 5) and ZnO (Ref. 6) doped with different transition metals (TM) (Co, Mn, Fe, Ni, Cr,…) have been the focus of much recent interest. Magnetic properties of doped ZnO have also been theoretically investigated by other authors[7] suggesting the existence of FM ordering without additional charge carriers for V, Cr, Fe, Co, and Ni dopants.

In spite of the number of papers published the situation is far from being well understood and there is no clear agreement about the origin of the magnetic behavior observed in most of the cases (see Ref. 8 for a summary). Extrinsic effects, such as ferromagnetic precipitates and impurity phases are responsible for the FM detected in most cases. Conflicting results have been reported for Co-doped TiO_2. Earlier

works suggested segregation and the formation of Co clusters as the origin of the FM signal,[9] but more recent results seem to indicate the existence of intrinsic FM.[10]

The same confusing situation also applies for Co-doped ZnO (Refs. 11–13) but recently intrinsic room temperature FM in single phase Co-doped[14,15] and Mn-doped[16] ZnO have been reported. It is worth mentioning that in these three cases relative low temperature ($\leqslant 400°-500°$) synthesis has been used for the preparation of the FM samples avoiding clustering and the formation of secondary phases.

In a previous work[17] we have reported that a close correlation can be established between the microstructure and magnetic properties of 5% molar CoO-doped ZnO nanoparticles. In the present work we report on the magnetic and structural properties of $Zn_{1-x}Co_xO$ (x between about 2% and 10%) nanophase particles prepared by the vaporization-condensation method in a solar reactor. We show that the appearance of the ferromagnetic ordering is intimately related to the microstructure of the samples, that can be tuned by changing the preparation conditions. Samples prepared in low pressure conditions (≈ 10 Torr) have a very homogeneous microstructure and are FM at low temperature and superparamagnetic at room temperature. They exhibit hysteretic behavior with low coercivity (about 300 Oe at $T=10$ K) and extrapolated zero-field magnetization well below that expected for Co^{2+} in a tetrahedral crystal field ($3\mu_B$/Co). On the other hand, samples prepared under pressure conditions ($\approx 70-100$ Torr) inside the evaporation chamber have a much faster growth process leading to a defective microstructure, as evidenced by transmission electron microscopy

(TEM) and high resolution electron microscopy (HREM), and are paramagnetic. This defective microstructure generates a nonhomogeneous distribution of Co atoms with a remarkable tendency to form Co-rich areas inside the ZnO matrix. Co-Co distances in these Co-rich zones are short and they favor antiferromagnetic (AF) interactions. Under these circumstances increasing the Co content does not induce FM but reinforces AF interactions.

EXPERIMENT AND RESULTS

Co-doped ZnO nanophase particles have been prepared by the vaporization-condensation method in a evaporation chamber (a glass balloon) placed at the focus of a solar reactor in the High Flux Solar Facilities in Odeillo. The material is melted inside the evaporation chamber by using the sun heating power focused in the sample by means of a curve focusing mirror, vaporized, and then condensed. The shape of the particles as well as particle size distribution can be controlled by varying the atmosphere conditions inside evaporation chamber. Since inside the glass balloon there are no heaters or any other thing but the sample itself this is a very clean evaporation system that allows us to avoid any kind of cross contamination.

The targets have been prepared by using a mixture of ZnO and CoO powders (Aldrich, purity 99.99%) heated in the air at 1115 °C during 12 h to obtain ceramic pellets. Samples of ZnO with 2%, 5%, and 10% molar of CoO have been prepared with different pressure conditions inside the evaporation chamber. Namely, small air flux is mantained through the evaporation chamber and the pressure inside is controlled by pumping with a rotatory pump. We have prepared particles at two different pressures, with low pressure inside the chamber ($\approx$10 Torr) and with high pressure ($\approx$70–100 Torr). The purity of the $Zn_{1-x}Co_xO$ obtained particles have been tested by using x-ray diffraction (XRD), HREM, and electron energy loss spectroscopy (EELS). HREM images and EELS spectra were carried out using a FEG TEM Jeol 2010F operated at 200 kV (point to point resolution 0.19 nm), and Gatan Image Filter 2000 with 0.8 eV energy resolution, respectively. This implies that in optimum conditions Co contents of about 1% could be detected. Image simulations were performed using the EMS software package.[18] The magnetic properties of the samples have been studied by using a MPMS-XL7 SQUID (superconducting quantum interference device, Quantum design) magnetometer.

Irrespective of x and the pressure conditions inside the chamber no evidence of Co segregation or any other phase different from würtzite type ZnO have been found. In Fig. 1 we show XRD spectra for samples of 2%, 5%, and 10% nominally. It is evident that only the peaks corresponding to the ZnO würtzite (SG $P6_3mc$, a=0.32 nm, c=0.52 nm) structure are detected.

Electron microscopy techniques (TEM, HREM) have also been used to characterize particles. No traces of impurities or secondary phases have been detected. EELS analyses performed on several particles systematically exhibited a very weak signal at an energy loss $\sim$800 eV corresponding to the
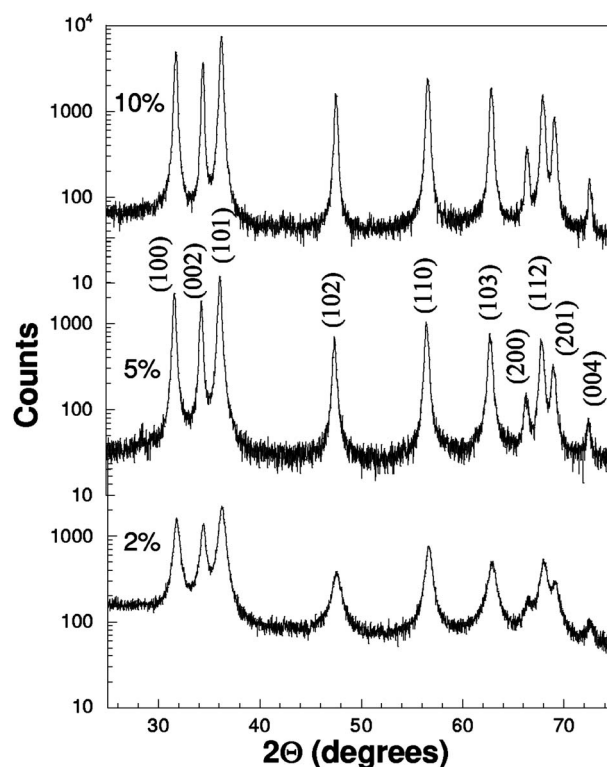

FIG. 1. X-ray diffraction patterns for samples with different Co content.

CoL peak. A typical example, corresponding to the 5% sample, is shown in Fig. 2. The inset is an enlarged view of the boxed area to illustrate the deviation of the background associated to the CoL feature. Quantitative processing of the spectra yielded an average Co concentration of about 4.5 at. %, thus indicating that Co^{2+} cations have been substituted for Zn^{2+} giving, within experimental accuracy, $Zn_{0.95}Co_{0.05}O$. Therefore, no Co containing foreign phases are expected. Moreover, no significant compositional differences between the rounded and tetrapodlike particles were detected.
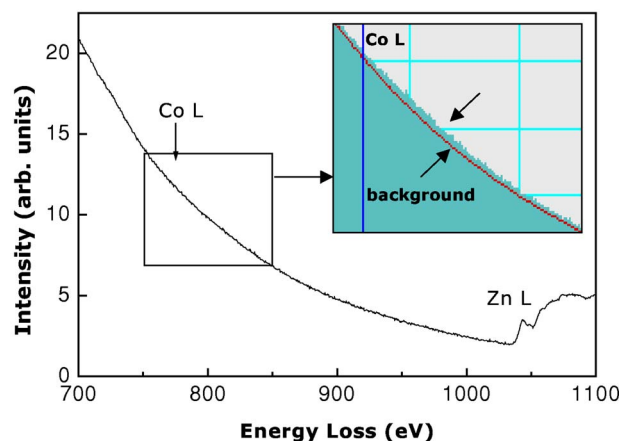

FIG. 2. (Color online) EELS spectrum for sample 1 (5% of Co prepared at low pressure). Inset: Magnified view of the boxed area to illustrate the deviation from the computed background, corresponding to the CoL peak.
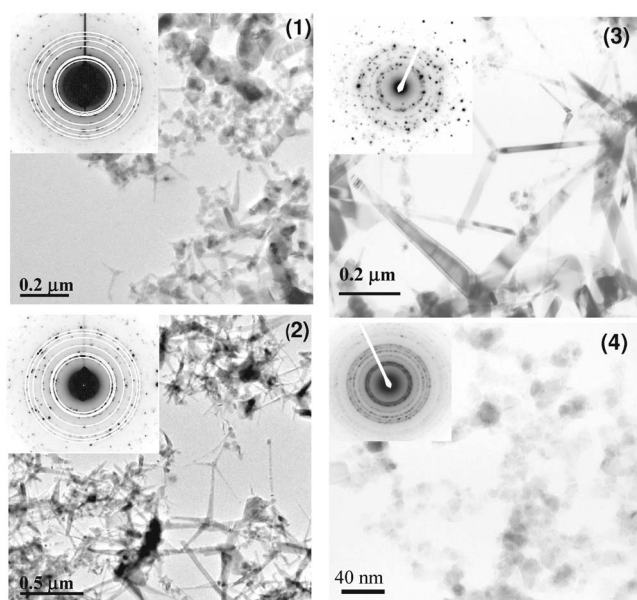
FIG. 3. (Left) TEM micrographs corresponding to samples with 5% of Co prepared with different pressure conditions inside the evaporation chamber: At low pressure (≈ 10 Torr) (1) and at high pressure ($\approx 70-100$ Torr) (2). Substantial differences in the size of the tetrapods are observed. Sample 1 also presents a significant fraction of rounded particles. Insets: Selected are diffraction (SAD) patterns of samples 1 and 2, respectively. Diffraction rings corresponding to the ZnO structure are indicated. (Right) TEM micrographs corresponding to samples with 10% of Co prepared at high pressure conditions (70–100 Torr) inside the evaporation chamber (3) and with 2% of Co at low pressure (≈ 10 Torr) (4). Insets: Selected are diffraction (SAD) patterns of samples 3 and 4, respectively.

Shape and size of the particles is modified by changing the pressure inside the evaporation chamber. In Fig. 3 (left) TEM micrographs corresponding to samples of 5% of Co prepared at low pressure (≈ 10 Torr) (sample 1) and at high pressure (70–100 Torr) (sample 2) are shown. Tetrapodlike morphologies are recognized in both cases. Similar structures have also been reported for Mn-doped samples.[19] Nevertheless, the size of the tetrapods are markedly larger when the synthesis is performed at higher pressures (sample 2). Therefore, we conclude that the growth rate along the axes of the tetrapod arms is enhanced at higher pressures. From HREM images it was deduced that the tetrapod arms are parallel to the [0001] direction. In addition, in sample 1 a large fraction of particles displaying non-tetrapod-like, mainly rounded, morphologies is also present. In Fig. 3 (right) we also show TEM micrographs corresponding to samples with 10% (sample 3) and 2% (sample 4) of Co. The same large tetrapodlike morphologies are found in sample 3 prepared under pressure conditions (70–100 Torr). Conversely in sample 4, prepared in vacuum conditions, only small rounded particles are found.

Selected area diffraction (SAD) patterns are also shown as insets in Fig. 3; in all the cases the diffraction rings corresponding to the würtzite ZnO structure are found. Although in agreement with XRD $\theta/2\theta$ patterns, SAD images typi-
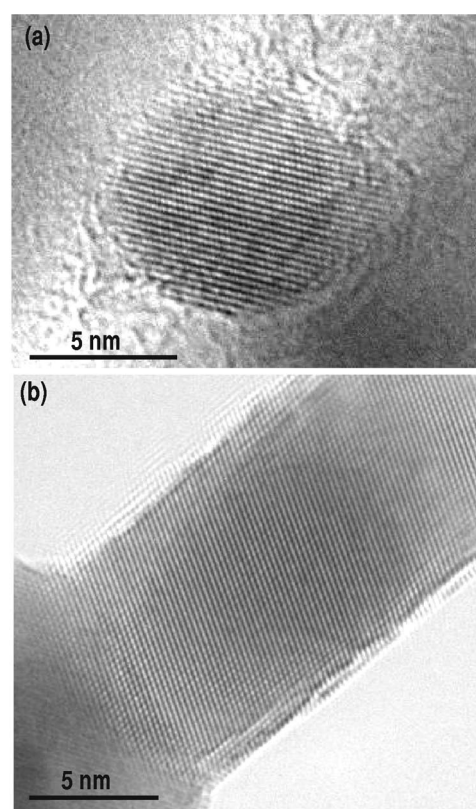

FIG. 4. HREM image of a rounded particle viewed along [20-2-1] (a) and a tetrapod arm [-1011] (b) corresponding to sample 1 [5% of Co at low pressure (10 Torr)]. A very homogeneous defects-free crystal structure is observed in both cases.

cally exhibit würtzite ZnO as the unique phase; highly exposed images taken on samples (2 and 3) revealed some very weak spots indicating that extremely small amounts of a foreign phase could be present in these cases. Unfortunately, careful inspection of highly exposed SAD images did not allow any conclusive results. Weak features appearing at ~0.202 nm and ~0.177 nm could indicate the presence of cubic Co. Spots at ~0.202 nm are also consistent with hexagonal Co and Co_3O_4 (or its isomorphs $CoCo_2O_4$ and $ZnCo_2O_4$), but for the latter possibility, they would correspond to the (004) weak reflection (19% of intensity relative to the strongest peak). The positions of most intense peaks of hexagonal Co and Co_3O_4 type oxides would overlap with ZnO rings thus precluding any conclusive insight into their occurrence in the present samples. Nevertheless, as we will see later, the paramagnetic behavior observed in both samples seems to preclude the occurrence of any FM foreign phase.

The growth rate of particles is controlled by changing the pressure inside the evaporation chamber and it also has a very strong effect on the microstructure of the samples. In Fig. 4 we present high resolution images of a rounded particle viewed along [20-2-1] (a) and a part of a tetrapod arm viewed along [-1011] (b) both corresponding to sample 1. In both cases, the images exhibit homogeneous, defect free crystalline structures with crystal lattices corresponding to ZnO. The contrast variation observed in the image of the
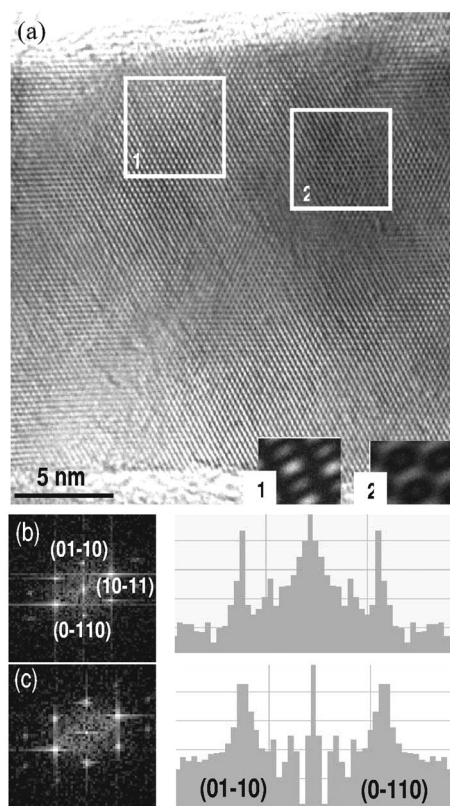
FIG. 5. (a) HREM image of a tetrapod arm corresponding to sample 2 (5% of Co prepared at higher pressure conditions) viewed along [-1011]. Insets 1 and 2 at the bottom of the image correspond to image simulations of pure ZnO and 10% Co substituted ZnO, respectively. Fast Fourier transform (FFT) spectra taken from boxed areas 1 and 2 are shown in (b) and (c), respectively. Intensity profiles taken across the (01-10) and (0-110) pairs of spots in the FFTs are included.

FIG. 6. (Color online) $M(H)$ curves obtained at $T = 10$ K for samples 1 to 4. The ferromagnetic character of samples prepared at low pressure (samples 1 and 4) is evident.

tetrapod arm [Fig. 4(b)] is associated to a thickness variation.

Conversely, HREM images corresponding to samples 2 and 3 indicate that defective structures develop within the tetrapod arms, likely to be the result of the higher growth rate of the crystallites. An example corresponding to sample 2 is shown in Fig. 5(a). The picture shows a part of a tetrapod arm viewed along the [-1011] direction. The image exhibits a patchedlike contrast distribution. The two boxed areas labeled 1 and 2 correspond to regions exhibiting different contrast behavior. In order to check the possibility that the origin of these contrast variations is associated with fluctuations in the concentration of Co, image simulations were carried out for pure ZnO and $Zn_{0.9}Co_{0.1}O$. Results are shown as insets in Fig. 5(a). The simulation of the ZnO phase reproduces the image in the boxed area labeled 1, while the substitution of 10% of Zn atoms by Co causes a marked weakening of the image contrast similar to that found in boxed area 2. Although the precise concentration of Co is very difficult to evaluate, the present results strongly suggest that the contrast variations found in images corresponding to sample 2 are caused by Co concentration fluctuations. The Fourier transform patterns shown in Figs. 5(b) and 5(c) were tak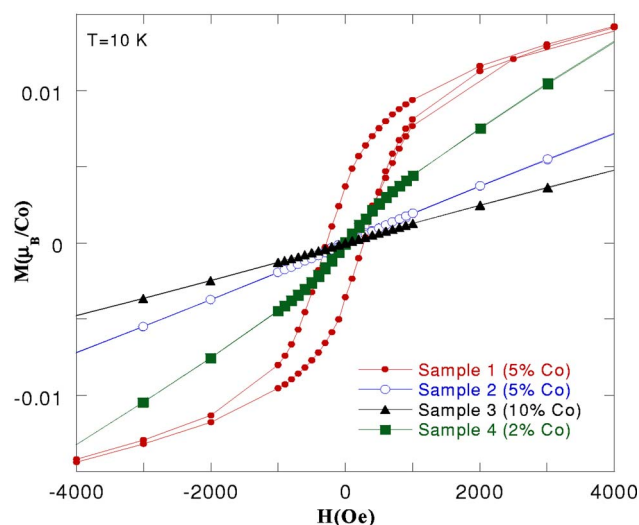en from boxed areas 1 and 2, respectively. The intensity profiles taken across the (01-10) and (0-110) pairs of spots are also shown. It can be clearly observed that the width of the intensity distribution around the spots is larger in boxed area 2, thus signaling the occurrence of slightly strained regions within the matrix. Such weak stress sources can be tentatively attributed to Co rich areas within the ZnO matrix. The small size of these areas, <5 nm, together with the small signal of Co in the EELS spectrum, precludes a quantitative confirmation of this mechanism. However, the fact that the intensity profiles shown in Figs. 5(b) and 5(c) only exhibit a variation on the width of the intensity distribution—but no definitive peak shift is observed—is consistent with the close similarity of the Co^{2+} and Zn^{2+} ionic radii (0.58 and 0.6 Å, respectively[20]). Our results strongly suggest that the occurrence of such defective regions is clearly associated with the higher growth rates of the crystallites grown at higher pressures.

The magnetization curves $[M(H)]$ at low temperature ($T = 10$ K) of samples 1 to 4 are shown in Fig. 6. It is evident from the figure that samples prepared at low pressure are FM at low T while those prepared at high pressure conditions are paramagnetic. In Fig. 7 the temperature dependence of the magnetic susceptibility $\chi(T)$ after a zero-field cooling-field cooling (ZFC-FC) process for sample 1 is shown. This sample, prepared at low pressure and corresponding nominally to 5% of Co content, exhibits the most evident ferromagnetic features with relatively large cohercivity and remanence at low T. All magnetic data shown in the figures have been corrected for ZnO diamagnetic contribution.[21]

ZFC-FC magnetization curves show the typical behavior of an assembly of superparamagnetic particles with irreversibility between the ZFC and FC branches of the magnetization below the blocking temperature T_B (see Fig. 7). As expected, T_B decreases when the magnetic field increases and ZFC and FC branches collapse for fields larger than about 2 kOe. This behavior is in agreement with the size of the $Zn_{1-x}Co_xO$ nanoparticles integrating the samples. Very similar ZFC-FC curves has been reported in Ref. 22, nevertheless
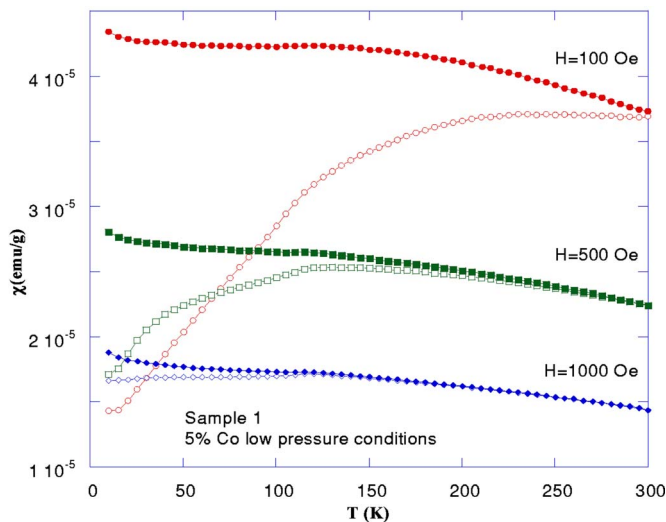
FIG. 7. (Color online) Thermal dependence of the magnetic susceptibility $[\chi(T)]$ of sample 1 obtained after a zero-field cooling-field cooling (ZFC-FC) process with an applied magnetic field of $H=100$ Oe.

they reflect a substantially different situation. In Ref. 22 the irreversibility is generated by the existence of Co clusters with a T_B well above room temperature (RT) as evidenced by the RT hysteresis loops with large coercivity (H_C) and remanence (MR). In our case $M(H)$ curves at 300 K and above exhibit the typical features of superparamagnetic behavior with negligible values of H_C and M_R. Further evidence of the superparamagnetic behavior at high temperature is presented in Fig. 8 where we depict M/M_S as a function of the temperature reduced field (H/T); the collapsing of the curves above 300 K confirms the superparamagnetic behavior.

Magnetization curves in the superparamagnetic regime have been fitted by using the Langevin function $\mathcal{L}(\mu_P H/k_B T)$ (see inset of Fig. 8) according to

$$M = M_S \mathcal{L}(\mu_p H/k_B T) \qquad (1)$$

M_S being the saturation magnetization and μ_P the average magnetic moment per particle. The fittings shown in Fig. 8 give values of the average magnetic moment per particle about $\mu_P \approx 1.3 \times 10^{14} \mu_B$, that taking into account the nominal Co content of 5% and the cell volume of ZnO ($V \approx 47.3$ Å^3), and assuming spherical particles will imply particles of about 20 nm in diameter. This rough estimation is in agreement with the smaller particle sizes found in our samples as can be appreciated in Figs. 3 and 4. Nevertheless, we should mention that a broad particle size distribution exists in or samples with particle sizes well above that obtained from the fits. These results are a clear indication that the distribution of Co atoms through the ZnO matrix is not uniform as we have already seen in HREM images.

In Fig. 9 we show the temperature dependence of the magnetization in a 50 kOe field. It is evident that the Curie temperature of the ferromagnetic nanoparticles is well above RT but certainly smaller than that of metallic Co. It is also evident from Fig. 9 that a paramagnetic contribution appears superimposed to the FM one. This contribution is also present in $M(H)$ curves making the evaluation of the actual value of the saturation magnetization M_S difficult. Our most optimistic estimations render values of about $M_S \approx 0.03 \mu_B/$Co at $T=5$ K, values that are very much smaller than that expected for Co^{2+}($3\mu_B$) and that clearly indicates that only a fraction of the Co atoms participate in FM; the rest contribute to the observed paramagnetic signal or may even be AF coupled. It is interesting to mention here that this is a recurrent problem in almost all the results reported in the literature. To the best of our knowledge, all the papers reporting "intrinsic" FM in Co or Mn doped ZnO give values of M_S clearly smaller than that expected for Co^{2+} or Mn^{2+}.[14,15,19,23]

The thermal decrease of the magnetization has been fitted by using Eq. (2) where the effect of the applied field on the
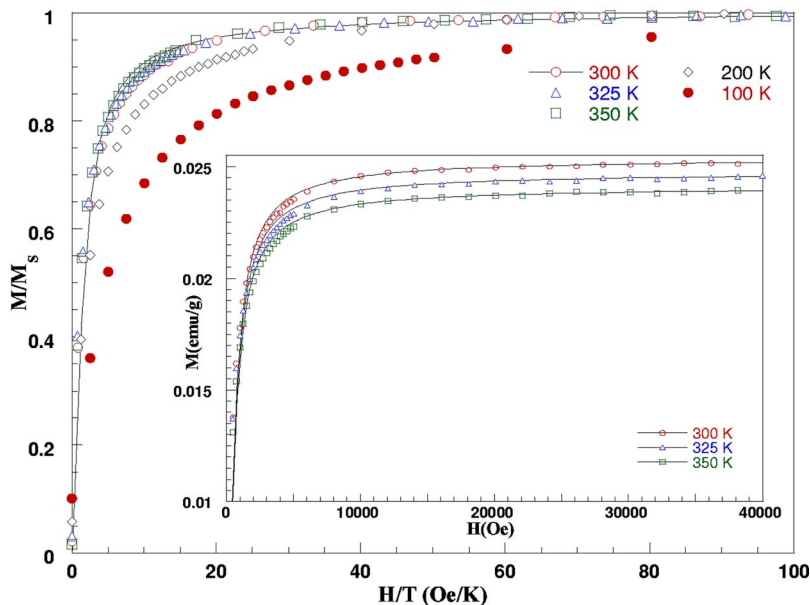

FIG. 8. (Color online) Normalized magnetization curves (M/M_S) as a function of the temperature reduced field (H/T). The superparamagnetic behavior of sample 1 at high temperatures ($T \geq 300$ K) is evidenced in this plot. Inset: Magnetization curves of sample 1 at high temperature. The lines are theoretical fits using Eq. (1) in the text.
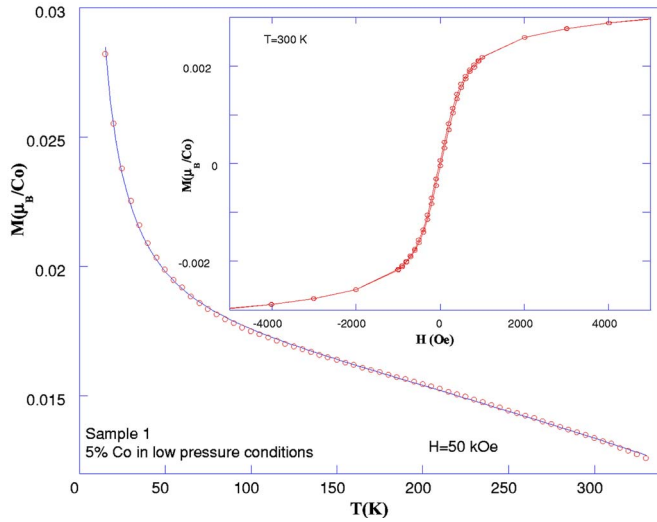
FIG. 9. (Color online) Temperature dependence of the magnetization of sample 1 in a magnetic field of $H=50$ kOe. Continuous line corresponds to the fitting by using Eq. (2) in the text. Inset: Hysteresis loop of sample 1 at room temperature.

spin wave spectrum has been taken into consideration:[24]

$$M(T) = H\chi_P(T) + M_S(1 - B[F(3/2, t_H)/\xi(3/2)]T^{3/2}), \quad (2)$$

where $\chi_P(T)=C/T$ is the paramagnetic susceptibility, C being the Curie constant, and M_S the saturation magnetization at $T=0$. The function $F(3/2, t_H)$ is given by the following expresion:[24]

$$F(3/2, t_H) \approx \xi(3/2) - (3.54/t_H^{1/2}) + (1.46/t_H) - (0.104/t_H^2)$$
$$+ (0.00425/t_H^3), \quad (3)$$

where $\xi(a)$ is the zeta function and, in particular, $\xi(3/2) = 2.612$ and $t_H = \mu_B H/k_B T$, μ_B being the Bohr magneton, and k_B the Boltzman constant. Equation (2) gives a very good reproduction of the experimental results (see Fig. 9). From the experimental fitting parameters we obtain that $M_S \approx 0.02\mu_B/\text{Co}$ [in close similarity with that obtained from $M(H)$ curves at low T] and $C = N\mu^2/3k_B \approx 1.11 \times 10^{-5}$ emu KOe^{-1} g^{-1} which give a value of the effective paramagnetic moment μ, of about $\mu \approx 0.1\mu_B/\text{Co}$. From the B parameter we can determine the spin wave stiffness constant D, that is related to B through the following equation:

$$B = 2.612(g\mu_B/M_S)[k_B/(4\pi D)]^{3/2}, \quad (4)$$

where g is the giromagnetic ratio. The value obtained for D from the fitting shown in Fig. 9 is $D \approx 6 \times 10^2$ meV Å^2. In a very naive picture D is related to the exchange integral J, through the expression $D = 2a^2 JS$,[25] $a(\approx 3.242$ Å) being the lattice parameter, and $S(=3/2)$ the magnetic moment. Substituting values we obtain that $J \approx 19$ meV. By using the mean field approximation $J \approx 3k_B T_C/[2zS(S+1)]$ we can estimate that the value of the magnetic transition temperature turns out to be about $T_C \approx 215$ K, assuming a uniform distribution of Co atoms ($z \approx 6 \times 5/100$).

The low values obtained for M_S, T_C, and μ give clear clues in the sense that the magnetic properties of TM-doped
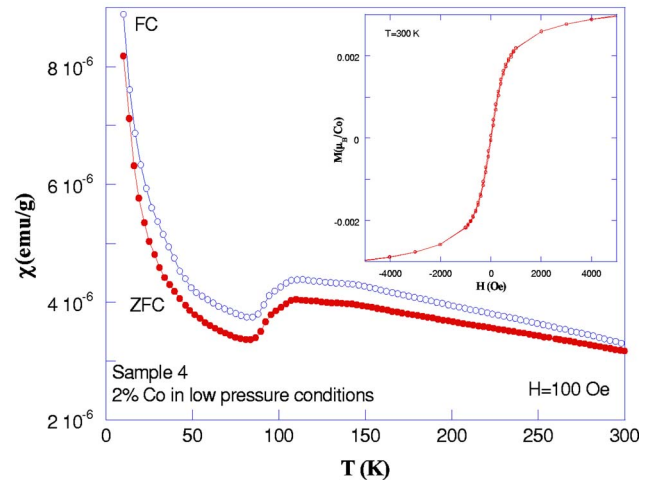

FIG. 10. (Color online) $M(T)$ curves obtained after a zero-field cooling-field cooling (ZFC-FC) process with an applied magnetic field of $H=100$ Oe corresponding to sample 4 (2% of Co in vacuum conditions). Inset: Hysteresis loop of sample 4 at room temperature.

ZnO cannot be explained by simply assuming a fully uniform distribution of Co atoms inside the ZnO matrix and it becomes evident that the FM ordering observed in these materials is still far from being well understood and deserves further studies both theoretical and experimental.

Ferromagnetic features are also found in sample 4 (2% of Co prepared at low pressure) (see Fig. 10), but in this case the values of M_S, H_C, and M_R are very much smaller than in sample 1 so we have centered our study to sample 1. In the main panel of Fig. 10 we show the temperature dependence of $\chi(T)$ after a ZFC-FC process under an applied field of 100 Oe. As in the case of sample 1 $\chi(T)$ curves show irreversibility between the ZFC and FC branches due to the blocking process of superparamagnetic particles. The effects of the blocking process become more evident close to T_B where the cusp of the susceptibility takes place and the superimposed paramagnetic contribution coming from paramagnetic Co atoms has substantially decreased. The inset shows the hysteresis loop at room temperature making evident the superparamagnetic behavior at high temperature.

On the other hand, samples prepared under high pressure conditions are paramagnetic (see Figs. 11 and 12). Sample 2 (5% Co prepared under pressure conditions) exhibits a Curie-Weiss behavior as evident in the inset of Fig. 11 where we depicted the inverse of susceptibility as a function of temperature for the FC branch under an applied field of $H = 100$ Oe. From the high temperature linear part a extrapolated Curie temperature of $\theta \approx -66$ K is obtained, which indicates that magnetic interactions between Co atoms are antiferromagnetic in nature. On the other hand, an effective paramagnetic moment of $\mu_{\text{eff}} \approx 1.4\mu_B/\text{Co}$ is determined, a value that is significantly different from that corresponding to Co^{2+} ($\mu_{\text{eff}} \approx 3.87\mu_B/\text{Co}$). It is also worth mentioning the existence of irreversibility between the FC and the ZFC branches of the susceptibility that should not exist in the case of a purely paramagnetic sample.

We have attempted to induce FM behavior in samples prepared under pressure conditions by increasing the Co con-
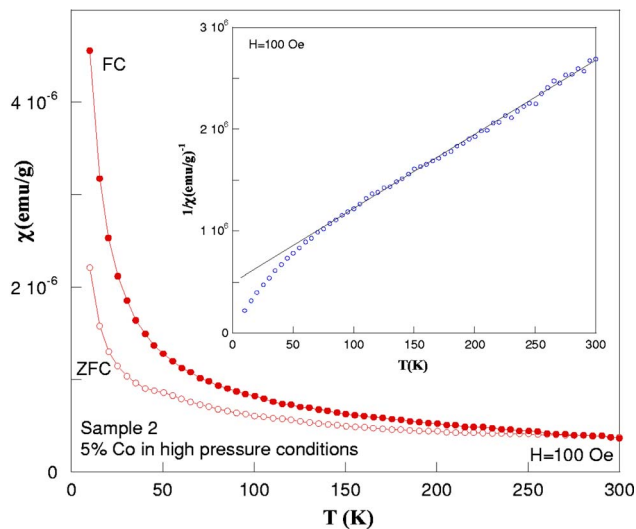
FIG. 11. (Color online) Thermal dependence of the susceptibility [$\chi(T)$] of sample 2 (5% of Co under high pressure conditions) after a ZFC-FC process in a magnetic field of $H=100$ Oe. Inset: Inverse of the FC branch of $\chi(T)$. The Curie-Weiss behavior of the susceptibility is evident.

tent. With this goal in mind we have prepared a series of samples containing 10% molar of CoO in the same high pressure conditions (sample 3). In spite of the increase of the Co content, samples prepared under pressure are still paramagnetic as shown in Fig. 12. Sample 3 also exhibits a Curie-Weiss behavior as evident in the inset of the figure where the $1/\chi(T)$ curve is depicted. From the high temperature linear part an extrapolated Curie temperature of $\theta \approx -180$ K is found, indicating a reinforcement of the AF when the Co content increases. An effective paramagnetic moment of $\mu_{\text{eff}} \approx 1.3 \mu_B/$Co is determined from the high temperature regime. The irreversibility between the FC and the
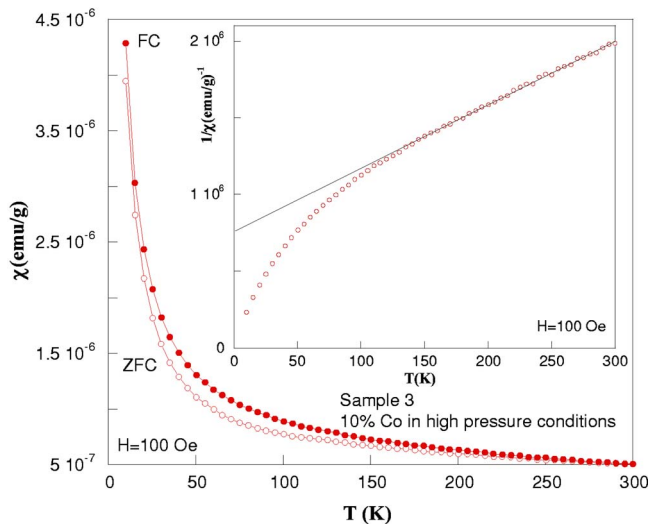

FIG. 12. (Color online) Thermal dependence of the susceptibility [$\chi(T)$] of sample 3 (10% of Co under high pressure conditions) after a ZFC-FC process in a magnetic field of $H=100$ Oe. Inset: Inverse of the FC branch of $\chi(T)$. The Curie-Weiss behavior of the susceptibility is evident.

ZFC branches of the susceptibility is also observed.

DISCUSSION AND CONCLUSIONS

The magnetic properties of DMS materials have been initially explained in terms of Dietl's model.[3] This model considers the FM to be mediated by delocalized or weakly localized holes in p-type materials. The spin-spin coupling is assumed to be a long range interaction, thus allowing the use of the mean field approximation based on the Ruderman-Kittel-Kasuya-Yosida (RKKY) interaction. In such circumstances the character [ferro or antiferromagnetic (AF)] of the magnetic interaction will depend on the Co atoms distance and therefore, the magnetic properties of DMS should be extremely sensitive to the TM content and to the microstructure, as it has been observed in several cases.[14,16,23]

In a nonhomogeneous mixture of Zn and Co atoms mean distances between Co atoms may vary randomly. Some Co atoms may be at shorter distance than others giving place to AF coupling, thus substantially reducing the overall magnetic moment. Another part may be at the right distances to promote FM interactions. Finally, some other Co atoms may be almost isolated exhibiting paramagnetic behavior. This would be a reliable source for the superimposed paramagnetic component observed in some measurements and would further reduce the contribution to M_S. On the other hand, in paramagnetic samples, as in the cases of samples 2 and 3, a tiny amount of Co atoms may still be giving a very small FM contribution, small enough to be undetected in $M(H)$ curves but that turns evident in ZFC-FC curves being responsible for the irreversibility observed in ZFC-FC processes in these samples.

With this picture in mind and the experimental results we have obtained for the different samples, a clear correlation may be established between the actual microstructure of the samples and the observed magnetic properties. While samples prepared at low pressure (≈ 10 Torr) (samples 1 and 4) exhibit a very uniform microstructure, samples prepared under high pressure conditions ($\approx 70-100$ Torr) (samples 2 and 3) irrespective to the Co content have a defective microstructure due to a much faster growth rate. HREM pictures make it evident that samples prepared at low pressure have a uniform microstructure giving place to a more homogeneous distribution of Co atoms. That implies that, assuming a mean field model (RKKY interactions), mean distances between Co atoms should favor FM interaction and the samples exhibit FM features. On the contrary, the defective microstructure observed in samples prepared at high pressure favors the formation of Co enriched areas inside the ZnO matrix (see Fig. 5) in which Co concentration is enlarged, therefore decreasing Co-Co distances and promoting AF interactions. The rest of the Co atoms not included in these Co enriched areas are far apart, giving place to the observed paramagnetic behavior, and also to a minute amount of FM responsible for the irreversibility observed in ZFC-FC susceptibility curves.

Very recently a mechanism has been proposed by Coey and co-workers[26] to explain the magnetic properties of diluted magnetic semiconductors. In this model FM exchange is proposed to be mediated by shallow donor electrons that

form bound magnetic polarons which overlap to create a spin-split impurity band. The magnetic phase diagram as a function of x obtained from this model includes regions of ferromagnetism, cluster paramagnetism, spin glass, and canted antiferromagnetism. Therefore, our experimental observations can also be understood in the framework of this model since the nonhomogeneous Co distribution in the samples will allow the existence of regions with different x and therefore different magnetic behavior.

In summary our results strongly indicate that intrinsic magnetic properties of Co-doped ZnO are intimately connected to the actual microstructure of the samples, i.e., magnetic properties can be tuned by the proper control of the preparation conditions. We have shown that Co-doped ZnO samples of very high purity without any impurity or secondary phases, as demonstrated by XRD, HREM, EELS, and TEM exhibit clearly different magnetic properties in close correlation with their microstructure. Our TEM studies show that, irespective of the Co content, particles of samples prepared at high pressure are larger than in samples prepared at low pressure due to a much faster growth rate. HREM studies demonstrate that faster growth rate implies a defective microstructure that generates a tendency to form Co-enriched zones in the ZnO matrix, i.e., distances between Co atoms in these zones are shorter reinforcing AF interactions. Co atoms not included in these areas are far apart and give place to the observed paramagnetic behavior.

Samples 1 and 4 exhibit a uniform microstructure, thus Co atoms are more uniformly distributed in the matrix and mean Co-Co distances favor FM interactions giving place to the observed FM ordering. Nevertheless, in a nonhomogeneous mixture some distances between Co atoms will be smaller than others and hence AF coupling may occur locally, reducing the overall magnetic moment. For the same reason some paramagnetic Co atoms may also exist, further reducing the observed M_S, and giving place to the observed paramagnetic contribution in $M(T)$ and $M(H)$ curves.

[1] See, for example, S. J. Pearton, C. R. Abernathy, D. P. Norton, A. F. Hebard, Y. D. Park, L. A. Boatner, and J. D. Budai, Mater. Sci. Eng., R. **R-40**, 137 (2003).

[2] H. Ohno, Science **281**, 951 (1998).

[3] T. Dietl, H. Ohno, M. Matsukura, J. Cibert, and D. Ferrand, Science **287**, 1019 (2000).

[4] S. A. Chambers, Mater. Today **5**, 34 (2002).

[5] Y. Matsumoto, M. Murakami, T. Shono, T. Hasegawa, T. Fukumura, M. Kawasaki, P. Ahmet, T. Chikyow, S. Koshikara, and H. Koinuma, Science **291**, 854 (2001).

[6] T. Fukumura, Z. Jin, A. Ohtomo, H. Koinuma, and M. Kawasaki, Appl. Phys. Lett. **75**, 3366 (1999).

[7] K. Sato and H. Katayama-Yosida, Semicond. Sci. Technol. **17**, 357 (2002).

[8] T. Fukumura, Y. Yamada, H. Toyosaki, T. Hasegawa, H. Koinuma, and M. Kawasaki, Appl. Surf. Sci. **223**, 62 (2004).

[9] P. A. Stamp, R. J. Kennedy, X. Yan, and J. S. Parker, J. Appl. Phys. **92**, 7114 (2002); S. A. Chambers, T. Droubay, C. M. Wang, A. S. Lea, R. F. C. Farrow, L. Folks, V. Deline, and S. Anders, Appl. Phys. Lett. **82**, 1257 (2003).

[10] S. R. Shinde, S. B. Ogale, S. Das Sarma, J. R. Simpson, H. A. Drew, S. E. Lofland, C. Lanci, J. P. Buban, N. D. Browning, V. N. Kulkarni, J. Higgins, R. P. Sharma, R. L. Greene, and T. Venkatesan, Phys. Rev. B **67**, 115211 (2003); A. Manivannan, G. Glaspell, and M. S. Seehra, J. Appl. Phys. **94**, 6994 (2003); T. Zhao, S. R. Shinde, S. B. Ogale, H. Zheng, T. Venkatesan, R. Ramesh and S. Das Sarma (unpublished).

[11] T. Fukumura, Z. Jin, M. Kawasaki, T. Shono, T. Hasegawa, S. Koshihara, and H. Koinuma, Appl. Phys. Lett. **78**, 958 (2001).

[12] S. W. Jung, S. J. An, Gyu-Chul Yi, C. U. Jung, Sung-Ik Lee, and Sunglae Cho, Appl. Phys. Lett. **80**, 4561 (2002).

[13] A. Tiwari, A. Kvit, D. Kumar, J. F. Muth, and J. Narayan, Solid State Commun. **121**, 371 (2002).

[14] L. Yan, C. K. Ong, and X. S. Rao, J. Appl. Phys. **96**, 508 (2004).

[15] S. Ramachandran, A. Tiwari, and J. Narayan, Appl. Phys. Lett. **84**, 5255 (2004).

[16] P. Sharma, A. Gupta, K. V. Rao, F. J. Owens, R. Sharma, R. Ahuja, J. M. Osorio Guillen, B. Johansson, and G. A. Gehring, Nat. Mater. **2**, 673 (2003).

[17] B. Martinez, F. Sandiumenge, Ll. Balcells, J. Arbiol, F. Sibieude, and C. Monty, Appl. Phys. Lett. **86**, 103113 (2005).

[18] P. Stadelmann, Ultramicroscopy **21**, 131 (1987).

[19] V. A. L. Roy, A. B. Djurisic, H. Liu, X. X. Zhang, Y. H. Leung, M. H. Xie, J. Gao, H. F. Lui, and C. Surya, Appl. Phys. Lett. **84**, 756 (2004).

[20] R. D. Shannon, Acta Crystallogr. **32**, 751 (1976).

[21] *CRC Handbook of Chemistry and Physics*, 80th ed., edited by D. R. Lide (CRC Press, Boca Raton, FL, 1999), pp. 4–134.

[22] Jung H. Park, Min G. Kim, Hyun M. Jang, Sangwoo Ryu, and Young M. Kim, Appl. Phys. Lett. **84**, 1338 (2004).

[23] A. Fouchet, W. Prellier, P. Padhan, Ch. Simon, B. Mercey, V. N. Kulkarni, and T. Venkatesan, J. Appl. Phys. **95**, 7187 (2004).

[24] F. Keffer, *Handbuch der Physick* (Springer-Verlag, Berlin, 1966), p. 28.

[25] C. Kittel, *Introduction to Solid State Physics* (Wiley, New York, 1986), p. 434.

[26] J. M. D. Coey, M. Venkatesan, and C. B. Fitzgerald, Nat. Mater. **4**, 173 (2005).